Pediatric Radiology (2022) 52:1826–1838
https://doi.org/10.1007/s00247-022-05377-9

THORACIC IMAGING

Pediatric large airway imaging: evolution and revolution

Mark C. Liszewski[1] · Pierluigi Ciet[2,3,4] · Abbey J. Winant[5] · Edward Y. Lee[5]

Received: 1 November 2021 / Revised: 26 February 2022 / Accepted: 1 April 2022 / Published online: 10 May 2022

Abstract
Infants and children often present with respiratory symptoms referable to the airway. For these pediatric patients, airway imaging is frequently performed to evaluate for underlying disorders of the large airway. Various imaging modalities have been used to evaluate the pediatric large airway, and pediatric airway imaging techniques have continued to evolve. Therefore, clear understanding of the status and new advances in pediatric large airway imaging is essential for practicing radiologists to make timely and accurate diagnoses, which can lead to optimal pediatric patient management.

Keywords Airway · Bronchi · Children · Computed tomography · Infants · Magnetic resonance imaging · Trachea

Introduction

Respiratory symptoms are a common indication for medical imaging of the neck and chest in children [1]. Large airway disorders are a frequent and important cause of pediatric respiratory symptoms, and high-quality airway imaging is essential for prompt and accurate diagnosis. Various imaging modalities, including radiography, fluoroscopy, CT and MRI, have been used to evaluate the large airway in children, and the roles of these complementary modalities have continued to evolve. Clear understanding of the status and new advances in pediatric large airway imaging is essential for practicing radiologists.

Therefore, in this article we first review the clinical utility and complementary roles that radiography, fluoroscopy, CT and MRI play in the evaluation of pediatric large airway disorders in current clinical practice, highlighting practical applications as well as novel innovations that are essential to the noninvasive diagnosis of various pediatric large airway disorders. In addition, we review commonly encountered congenital and acquired disorders of the pediatric large airway, including conditions causing static and dynamic abnormalities of the large airway.

Currently available imaging modalities and techniques

Four main imaging modalities that have been used for evaluating pediatric large airway disorders are radiography, fluoroscopy, CT and MRI. Among them, CT and MRI have undergone major imaging advances during the last two decades. The clinical utility of each of these imaging modalities for evaluating pediatric large airway disorders is briefly discussed in the following sections.

Radiography

Given its widespread availability and low cost, anteroposterior and lateral radiography of the neck and chest is the usual first-line imaging study for evaluating the large airway in the pediatric population. High-detail radiography of the large airway can be achieved using a magnified high kilovoltage (kV) technique in which the anteroposterior (AP) radiograph is tightly coned to the neck and selectively filtered to eliminate overlap from the cervical spine. In addition, the lateral

✉ Mark C. Liszewski
mliszews@montefiore.org

1 Departments of Radiology and Pediatrics, Montefiore Medical Center and Albert Einstein College of Medicine, 111 East 210th St., Bronx, NY 10467, USA

2 Department of Radiology and Nuclear Medicine, Erasmus MC–Sophia Children's Hospital, Rotterdam, The Netherlands

3 Department of Pediatric Respiratory Medicine, Erasmus MC–Sophia Children's Hospital, Rotterdam, The Netherlands

4 Department of Radiology, University Hospital of Cagliari, Cagliari, Italy

5 Department of Radiology, Boston Children's Hospital and Harvard Medical School, Boston, MA, USA

radiograph is obtained at end-inspiration with the neck in an extended position to optimize visualization of the large airway. Standard AP or posteroanterior (PA) and lateral radiographs of the chest can also be helpful for evaluating the lower large airway, and expiratory or lateral decubitus radiographs can be used when evaluating for the secondary signs of airway pathology, such as air trapping.

Fluoroscopy

Airway fluoroscopy can be used to detect changes in large airway caliber throughout the respiratory cycle in real time in order to diagnose conditions that lead to dynamic abnormalities of the large airway, such as tracheomalacia and bronchomalacia. Similar to radiography, the main benefit of fluoroscopy is its wide availability and relative low cost. Consequently, fluoroscopy has historically been used as a first-line imaging test for tracheomalacia and bronchomalacia. However, airway fluoroscopy has relatively lower sensitivity for detecting laryngotracheal pathology in children [2, 3] and is increasingly being replaced with CT and MRI as advances in cross-sectional imaging have allowed for these modalities to be used with increased frequency to evaluate dynamic conditions of the large airway in children [3–8], as discussed in the following sections.

Computed tomography

Currently, CT is the preferred noninvasive imaging test for evaluating the large airway in the pediatric population [5, 6]. Static abnormalities of the large airway are typically assessed with imaging performed at end-inspiration, whereas dynamic pathologies of the large airway can be assessed with paired end-inspiratory and end-expiratory imaging, cine CT during free breathing, or four-dimensional (4-D) CT during free breathing [4, 9, 10]. Paired end-inspiratory and end-expiratory imaging can only be performed in children who are able to follow breathing instructions or by utilizing controlled mechanical ventilation in children who are anesthetized. Therefore, cine CT or 4-D CT during free breathing must be used in non-anesthetized children who are unable to follow breathing instructions. Modern multidetector CT scanners, particularly those with higher row detectors, can achieve rapid scan times that produce images with minimal motion artifact, allowing for imaging of infants and young children without sedation [11].

Assessing for dynamic large airway disorders with paired inspiratory and expiratory CT requires intubation in infants and younger children who are unable to follow breathing instructions; however, paired inspiratory and expiratory CT can usually be obtained without sedation in older children [10, 12]. Newer cine CT and 4-D CT techniques can dynamically assess the pediatric large airway during free breathing and can be performed without sedation, even in infants and younger children [6, 13, 14].

The paired inspiratory and expiratory multidetector computed tomography (MDCT) imaging of the large airways can be obtained with MDCT scanners with more than four rows. Two dose are milliamperes (mAs) and kilovoltage peak (kVp) and can be adjusted based on age, weight or girth of the child [10] following the dose as low as reasonably achievable (ALARA) principle. A previous study showed that the radiation dose of a paired inspiratory and expiratory MDCT study can be reduced by 23% by decreasing milliamperes by 50% during the expiratory phase of MDCT imaging while maintaining similar diagnostic confidence for evaluating the tracheal lumen in pediatric patients [15]. Parameters for cine MDCT imaging of the large airways are based on low-dose mAs and kVp technique combined with fast gantry rotation time ($\leq$0.5 s), thin detector collimation (0.5–0.625 mm) and four contiguous cine data sets from a single acquisition and real-time review [15]. Parameters for dynamic 4-D MDCT imaging of the large airway include low-dose milliamperage (mA) as determined by the formula [(kg$\times$2.5)+5] / 0.35, 80 kVp, continuous scanning for 1.4 s (4 cycles at 350 ms/rotation), and imaging reconstructions of 8–10 phases of obtained CT data set for image review in real-time dynamic mode.

Although the large airway is often well assessed without intravenous contrast agent (because of the intrinsic contrast between air-filled airway and adjacent soft tissues), intravenous contrast agent is often added to evaluate the adjacent mediastinal structures and assess for the vascular anomalies that are associated with large airway narrowing [10, 16]. Although CT has the advantage of producing high-detail cross-sectional images of the large airway and adjacent thoracic structures, often without the need for sedation, the major disadvantage of CT is exposure to ionizing radiation in this vulnerable patient population. In addition, multiphase dynamic CT imaging does increase the ionizing radiation dose. To reduce radiation dose, careful consideration of the technical CT parameters, such as reducing the mA on expiratory CT images, is typically recommended [15]. Careful clinical consideration of the risks and benefits of imaging with modalities that use ionizing radiation is important, and alternative imaging modalities should be considered, although they might decrease diagnostic yield.

Magnetic resonance imaging

Magnetic resonance imaging has been widely adopted as a preferred imaging modality in the pediatric population because of its superior contrast resolution and lack of ionizing radiation. However, imaging of the large airway with MRI presents challenges because of the limited signal from aerated lung, motion artifact and signal dephasing at air–tissue interfaces [17]. Advances in MR scanner technology, such as the development of less motion-sensitive sequences utilizing radial and helicoidal k-space acquisitions (to decrease motion artifact), have improved large airway imaging quality, allowing MRI of the large airway to be possible [7]. MRI is now used for evaluating the large airway

in children at many pediatric institutions with specialized expertise and is beginning to be adopted widely.

In young children who are unable to follow breathing instructions, anesthesia is generally required for MR imaging of the large airway, and the risks of anesthesia must be weighed against the benefits of avoiding ionizing radiation [18]. Older children who can follow breathing instructions can often complete the MRI without anesthesia, and preparation with coaching and simulation prior to the exam greatly improves the likelihood of success [18, 19].

Magnetic resonance imaging airway protocols can be divided into static protocols, which are optimized for evaluating fixed abnormalities of the large airway, and dynamic protocols, which are optimized for evaluating large airway abnormalities that change during the respiratory cycle. Suggested MRI static and dynamic airway imaging protocols are presented in Tables 1, 2 and 3. Contrast-enhanced MR sequences can be helpful depending on the indication, and contrast or non-contrast MR angiography should be performed when evaluating for the presence of a vascular ring [20].

Technological advancements in large airway imaging

The development of CT revolutionized diagnostic imaging evaluation of the pediatric airway by providing a noninvasive imaging modality that is highly sensitive and specific for pediatric large airway disorders [5, 10]. With development of multidetector CT scanners, with higher numbers of detectors and faster gantry rotation times, modern CT scanners can essentially freeze motion, allowing for pediatric large airway

Table 1 Static MRI airway imaging protocol

Sequence	Imaging plane	Voxel resolution (mm^3)
3-D breath-hold PD T1-W RF spoiled GRE FSPGR (LAVA), FLASH (VIBE), T1-FFE (THRIVE)	Axial, coronal or sagittal	Min 3.0×3.0×3.0 Max 1.5×1.5×1.5
2-D breath-hold/free-breathing T1/T2 single-shot steady-state GRE FIESTA, TrueFISP, balanced FFE	Axial, coronal or sagittal	Min 3.0×3.0×7.0 Max 1.5×1.5×4.0
2-D free-breathing (Nav/RT/Avg) PD T2-W FS FSE (PROPELLER, BLADE, MultiVane XD)	Axial	Min 1.0×1.0×5.0 Max 0.7×0.7×2.0
3-D free-breathing (Nav/RT) PD T1-W UTE, ZTE	Axial, coronal or sagittal	Min 1.5×1.5×1.5 Max 0.8×0.8×0.8
3-D free-breathing (Nav/RT) T2-W FS FSE (CUBE, SPACE, VISTA)	Axial, sagittal	Min 1.5×1.5×1.5 Max 0.8×0.8×0.8

2-D two-dimensional, *3-D* three-dimensional, *Avg* free-breathing with multiple averaging, *FFE* fast field echo, *FIESTA* fast imaging employing steady-state acquisition, *FLASH* fast low-angle-shot magnetic resonance imaging, *FS* fat suppressed, *FSE* fast spin echo, *FSPGR* fast spoiled gradient recalled echo, *GRE* gradient recalled echo, *LAVA* liver acceleration volume acquisition, *Nav* navigated, *PD* proton density, *PROPELLER* periodically rotated overlapping parallel lines with enhanced reconstruction, *RF* radiofrequency, *RT* respiratory-triggered, *SPACE* sampling perfection with application-optimized contrasts using different flip angle evolution, *T1-W* T1-weighted, *T2-W* T2-weighted, *THRIVE* T1 high-resolution isotropic volume excitation, *TrueFISP* true fast imaging with steady-state precession, *UTE* ultrashort echo time, *VIBE* volumetric interpolated breath-hold examination, *VISTA* volume isotropic turbo spin-echo acquisition, *ZTE* zero echo time

Table 2 Dynamic MRI airway imaging protocol

Sequence	Imaging plane	Voxel resolution (mm^3)
4-D (PD-T1-W) multiphase RF-spoiled 3-D GRE (TRICKS-DISCO, TWIST-GRASP, 4D-TRAK)	Axial, coronal or sagittal	Min 3.0×3.0×3.0 Max 2.0×2.0×2.0
2-D multiphase (T1/T2) steady-state balanced GRE FIESTA, TrueFISP, balanced FFE	Axial, coronal or sagittal	Min 1.5×1.5×4.0 Max 1.0×1.0×2.0
4-D retrospective free-breathing (PD T1-W) multiphase UTE	Axial, coronal or sagittal	Min 1.5×1.5×1.5 Max 0.7×0.7×0.7
4-D retrospective free-breathing (PD T1-W) multiphase ZTE	Axial, coronal or sagittal	Min 1.5×1.5×1.5 Max 0.8×0.8×0.8

3-D three-dimensional, *4-D* four-dimensional, *DISCO* differential sub-sampling with Cartesian ordering, *FFE* fast field echo, *FIESTA* fast imaging employing steady-state acquisition, *GRASP* golden-angle radial sparse parallel, *GRE* gradient recalled echo, *PD* proton density, *RF* radiofrequency, *T1-W* T1-weighted, *T2-W* T2-weighted, *TRAK* time-resolved angiography using keyhole, *TRICKS* time-resolved imaging of contrast kinetics, *TrueFISP* true fast imaging with steady-state precession, *TWIST* time-resolved angiography with interleaved stochastic trajectories, *UTE* ultrashort echo time, *ZTE* zero echo time

Table 3 Detailed MRI airway imaging sequences

Sequence	SPGR 3-D BH	UTE 3-D	ZTE 3-D vnav	ZTE 4-D	ZTE 3-D breath-hold	PROPELLER
Acquisition plane	Sagittal	Axial	Axial	Coronal	Coronal	Axial
TR/TE (ms)	1.5/0.6	5.2/0.032	1.1/0	1.4/0	1.25/0	–[a]/73
Flip angle (°)	2	3	2	1	2	90/120
Radiofrequency	Selective	Selective	Non-selective	Non-selective	Non-selective	Selective
In-plane matrix	120×120	228×228	200×200	150×150	150×150	340×340
k-space trajectory	Cartesian	Cones	Radial	Radial	Radial	Radial blades
Echo train length	–	–	–	–	–	14
In-plane FOV	36	34	30	34	34	34
Rectangular FOV	0.75	–	–	–	–	–
No phase wrap	–	–	–	–	–	1.4
Actual voxel resolution (mm^3)	3.0×3.0×3.0 130	1.5×1.5×1.5 230	1.5×1.5×1.5 200	2.2×2.2×2.2 110	2.2×2.2×2.2 110	1.0×1.0×3.5 50–70
Slices Slice thickness	3.0	1.5	1.5	2.2	2.2	3.5
Receiver bandwidth (KHz)	100 90 90	125	62.5	50	62.5	83.33
Parallel imaging (ARC)	None 1.5×1.2 1.5×1.2	None	None	None	None	3.0
Number of averages	1	1	2.5	7	1	2.0
Number of phases	1	1	1	16	1	1
No. of spokes per segment	–	–[b]	900	64	200	14
Physiological triggering	BH	Prospective pneumobelt	Prospective projection navigator	Retrospective pneumobelt	BH	Prospective projection navigator
Acceptance window	–	–	2.0 mm	–	–	2.0 mm
Scan time (s) RR = 20	13 s 8 s 5–6 s×2 BH	4 min 48 s	9 min 50 s	3 min 10 s	20 s	5 min 5 s[c]

ARC auto-calibrating reconstruction for Cartesian sampling, *BH* breath-hold, *FOV* field of view, *PROPELLER* periodically rotated overlapping parallel lines with enhanced reconstruction, *RR* respiratory rate, *SPGR* spoiled gradient echo, *TE* echo time, *TR* repetition time, *UTE* ultrashort echo time, *ZTE* zero echo time

[a] Respiratory gated scan with usually long TR

[b] Depending on respiratory rate

[c] Respiratory rate = 26

imaging without anesthesia in most cases. Novel cine CT and 4-D dynamic multiphase CT now provide sensitive and specific diagnostic imaging tools that can detect dynamic large airway disease, without an invasive test (e.g., bronchoscopy) [14, 16, 21]. The major advantages of CT must be weighed against the risk of ionizing radiation, which is potentially more harmful in children.

Magnetic resonance imaging provides the benefit of a cross-sectional imaging modality with excellent contrast resolution that, unlike CT, does not require ionizing radiation. This main benefit has led to the latest evolution of pediatric airway imaging: the development of MRI for the static and dynamic evaluation of the pediatric large airway [7, 22, 23]. The development of ultrafast MR imaging sequences has begun to address motion artifact, the main impediment to high-quality diagnostic MR evaluation of the pediatric large airway [7, 22, 23]. Ultrafast MR sequences reduce the need for anesthesia and have led to the development of cine MRI, providing a radiation-free alternative to evaluate the pediatric airway [7, 22, 23]. Currently only available in centers with specific expertise, MRI is likely be more widely used to evaluate the pediatric large airway as ultrafast MR imaging techniques become more widely available.

Spectrum of pediatric large airway disorders

Static imaging evaluation

Congenital large airway malformations

Congenital malformations that result in fixed anomalies of the large airway can be assessed with static imaging

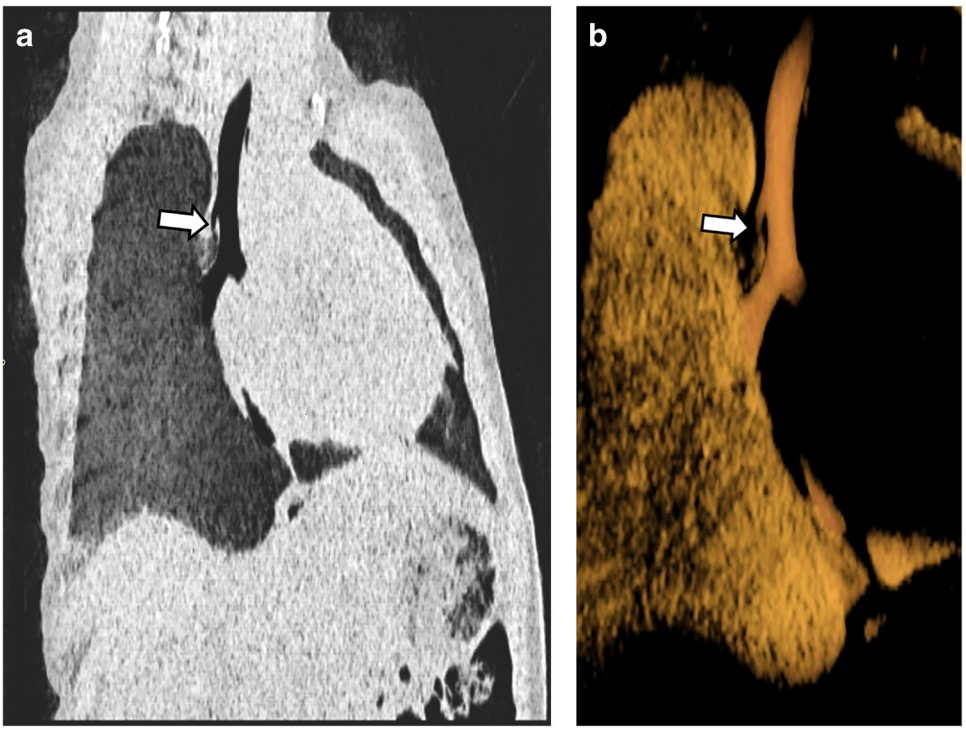

Fig. 1 Tracheal bronchus in a 10-month-old girl who presented with respiratory distress and recurrent right upper lobe atelectasis. Subsequently obtained bronchoscopy confirmed the diagnosis of tracheal bronchus. **a** Sagittal oblique minimum-intensity projection CT image shows an anomalous right upper lobe bronchus (*arrow*) directly arising from the trachea above the carina. **b** Anterior view of 3-D-volume rendered CT image confirms an anomalous right upper lobe bronchus (*arrow*), also known as tracheal bronchus

protocols. The most commonly encountered fixed congenital malformations include tracheobronchial branching anomalies, congenital tracheobronchial stenosis, bronchial atresia, and airway narrowing from extrinsic compression (i.e. vascular rings or pulmonary sling) [7, 8].

Tracheobronchial branching anomalies

Examples of tracheobronchial branching anomalies include tracheal bronchus, bridging bronchus, esophageal bronchus and cardiac bronchus [5, 6]. *Tracheal bronchus* is an anomalous segmental bronchus that arises from the trachea (Fig. 1). A tracheal bronchus might be a displaced bronchus, supplying a normal segment of the tracheobronchial tree; a supernumerary bronchus, existing in addition to a normally segmented tracheobronchial tree; or a rudimentary bronchus, with a blind-ending termination [9, 24, 25]. Tracheal bronchus is most often asymptomatic but occasionally causes recurrent atelectasis, pneumonia and hemoptysis [8]. *Bridging bronchus* is an anomalous bronchus that crosses the midline, is associated with pulmonary sling, and is frequently narrowed by congenital stenosis (due to tracheal rings), bronchomalacia or extrinsic compression from pulmonary sling [25, 26] (Fig. 2). Symptoms associated with bridging bronchus include respiratory distress and stridor. *Esophageal bronchus* is an anomalous bronchus that arises from the esophagus and typically presents in the neonatal period with severe aspiration caused by esophageal contents directly entering the lung (Fig. 3). Symptoms associated with esophageal bronchus are typically related to aspiration of ingested material and include cough and respiratory distress after eating and recurrent aspiration pneumonia. *Cardiac bronchus* is a supernumerary bronchus that typically originates from the right main bronchus or bronchus intermedius and travels in parallel with the bronchus intermedius toward the pericardium. Cardiac bronchus might end blindly or terminate in disorganized parenchyma, cystic spaces or an aerated lobule. Cardiac bronchus is often asymptomatic but is sometimes associated with pneumonia.

Congenital tracheobronchial stenosis

Congenital tracheobronchial stenosis is a rare condition in which the tracheal or bronchial diameter is reduced by greater that 50% [27] (Figs. 4 and 5). Stenosis can be focal or over a long distance and might be associated with cartilaginous rings. Affected pediatric patients might present with symptoms of respiratory distress and stridor and are frequently misdiagnosed with asthma until a correct diagnosis is made [28]. CT is the imaging test of choice for diagnosing congenital tracheobronchial stenosis, although MRI is being used in centers with expertise [27]. CT can also provide follow-up evaluation after surgical repair or stent placement (Fig. 6). On imaging of congenital tracheobronchial stenosis, the large airway narrowing is fixed throughout the respiratory cycle and can be differentiated from tracheobronchomalacia with inspiratory/expiratory imaging or cine imaging [23].

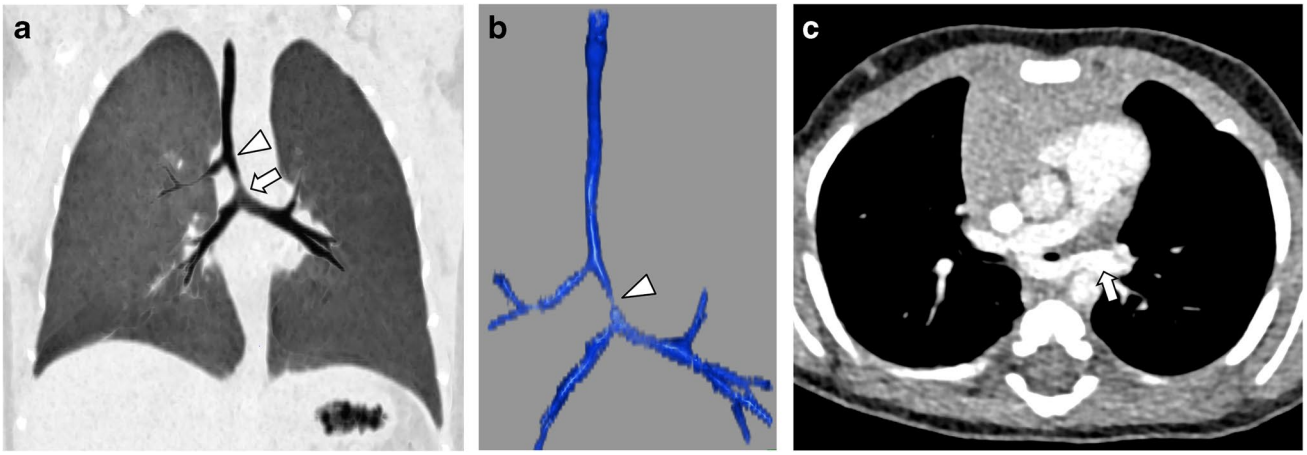

Fig. 2 Bridging bronchus in a 5-month-old girl who presented with shortness of breath and was found to have a pulmonary artery sling. **a** Coronal minimum-intensity projection CT image shows carina (*arrowhead*) and pseudocarina (*arrow*) in addition to bridging bronchus, which is an anomalous bronchus that crosses the midline. The caliber of the bronchus between the carina and pseudocarina is small because of underlying congenital stenosis, frequently due to tracheal rings. **b** Anterior 3-D-volume rendered CT image better demonstrates the entire extent and narrowing (*arrowhead*). **c** Axial enhanced CT image shows an anomalous left pulmonary artery (*arrow*) arising from the main pulmonary artery and crossing the midline to the left, consistent with a pulmonary artery sling

Bronchial atresia

Bronchial atresia is a condition in which a segmental bronchus is focally occluded and the lung distal to the atresia is isolated from the tracheobronchial tree. The interruption of the bronchus causes mucus to collect within the airway distal to the atresia, forming a bronchocele [25]. The lung distal to the atresia is typically aerated via collateral pathways of aeration (e.g., pores of Kohn and channels of Lambert), resulting in air-trapping and hypoxia-mediated oligemia, which further leads to hyperlucent lung surrounding the bronchocele [7]. Bronchocele and hyperlucent surrounding lung segment might be first detected on radiographs; however, diagnosis is typically confirmed with CT (Fig. 7). MRI can be used as an alternative to CT in centers with expertise. In particular, the characteristic bronchocele is typically well-visualized on T2-weighted MR sequences as a tubular T2-hyperintense structure, with relative hypointense signal in the surrounding pulmonary segment [7] (Fig. 7). Bronchial atresia can occur on a spectrum with other congenital lung lesions including bronchopulmonary sequestration; therefore, CT and MRI might be performed with contrast agent, and CT angiography and MR angiography protocols are sometimes combined with airway protocols to evaluate the underlying vascular anatomy [29].

Vascular rings and sling

Fixed large airway narrowing is sometimes caused by extrinsic compression from entities such as congenital vascular rings and pulmonary sling. Examples of vascular rings include double aortic arch, right aortic arch with aberrant

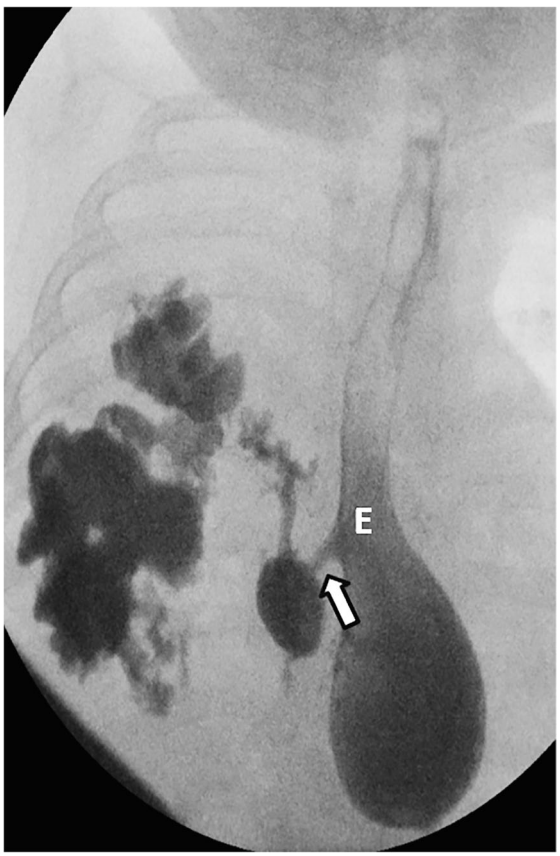

Fig. 3 Esophageal bronchus in a 6-month-old girl who presented with recurrent cough, fever, gagging with feeds, and right lung pneumonia. Posteroanterior fluoroscopy image from upper gastrointestinal study with oral contrast agent shows a direct communication (*arrow*) between the esophagus (*E*) and a bronchus, which communicates with a right lower lobe bronchopulmonary malformation. Also note the distal esophageal stenosis

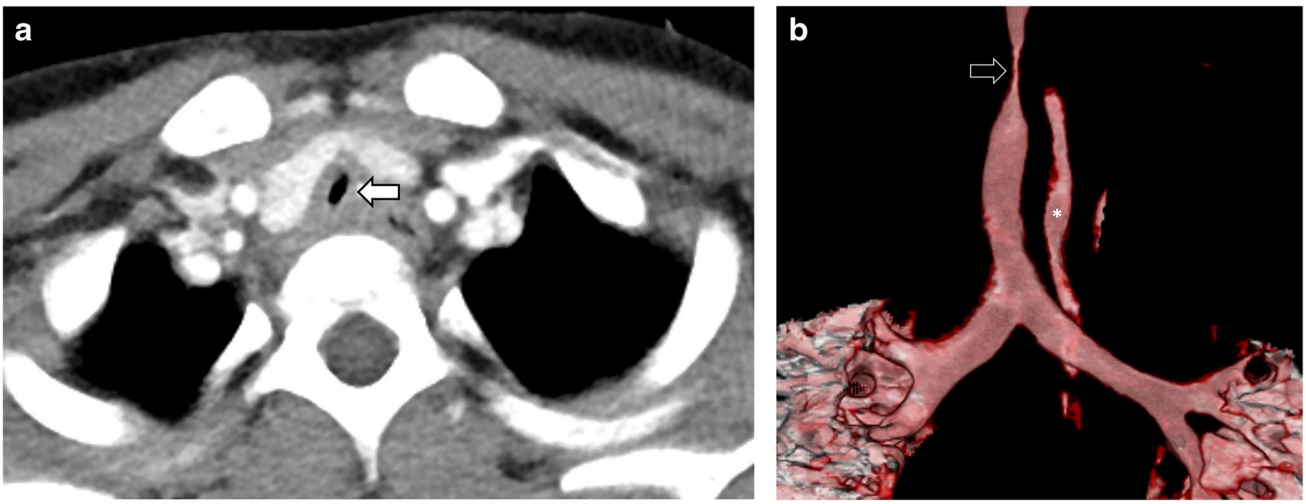

Fig. 4 Congenital tracheal stenosis in a 5-year-old boy who presented with progressively worsening shortness of breath. Subsequently obtained bronchoscopy confirmed the diagnosis of tracheal stenosis. **a** Axial enhanced CT image at the level of upper intrathoracic trachea shows a marked narrowing (*arrow*). **b** Anterior 3-D-volume rendered CT image better demonstrates the degree and extent of the congenital tracheal stenosis (*arrow*). Of note, gaseous distension of the esophagus (*asterisk*) is also partially visualized

left subclavian artery, cervical aortic arch, and left aortic arch with right descending aorta and right ligamentum arteriosum, which is often inferred by the presence of a diverticulum [30] (Fig. 8). Pulmonary sling is characterized by the left main pulmonary artery originating from the right pulmonary artery (instead of the main pulmonary artery), with the anomalous left pulmonary artery typically compressing the large airway [26, 31] (Fig. 2). In addition, intrinsic large airway narrowing and branching anomalies are frequently associated with pulmonary sling [26, 31].

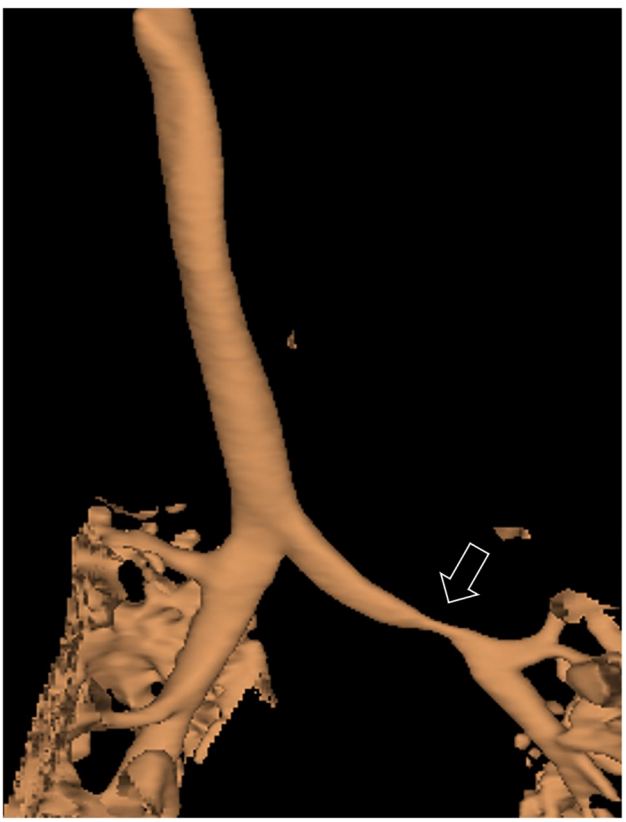

Fig. 5 Congenital bronchial stenosis in a 2-month-old girl who presented with respiratory distress. Anterior 3-D-volume rendered CT image shows a short segment of marked narrowing (*arrow*) involving the distal left mainstem bronchus

Fig. 6 Stent placement for congenital stenosis in the left main bronchus in a 9-year-old girl with recurrent bronchial stenosis despite balloon dilatation procedure. Coronal enhanced CT image shows a metallic stent (*arrow*) in the proximal to mid left main bronchus. The metallic stent patency can be evaluated with CT

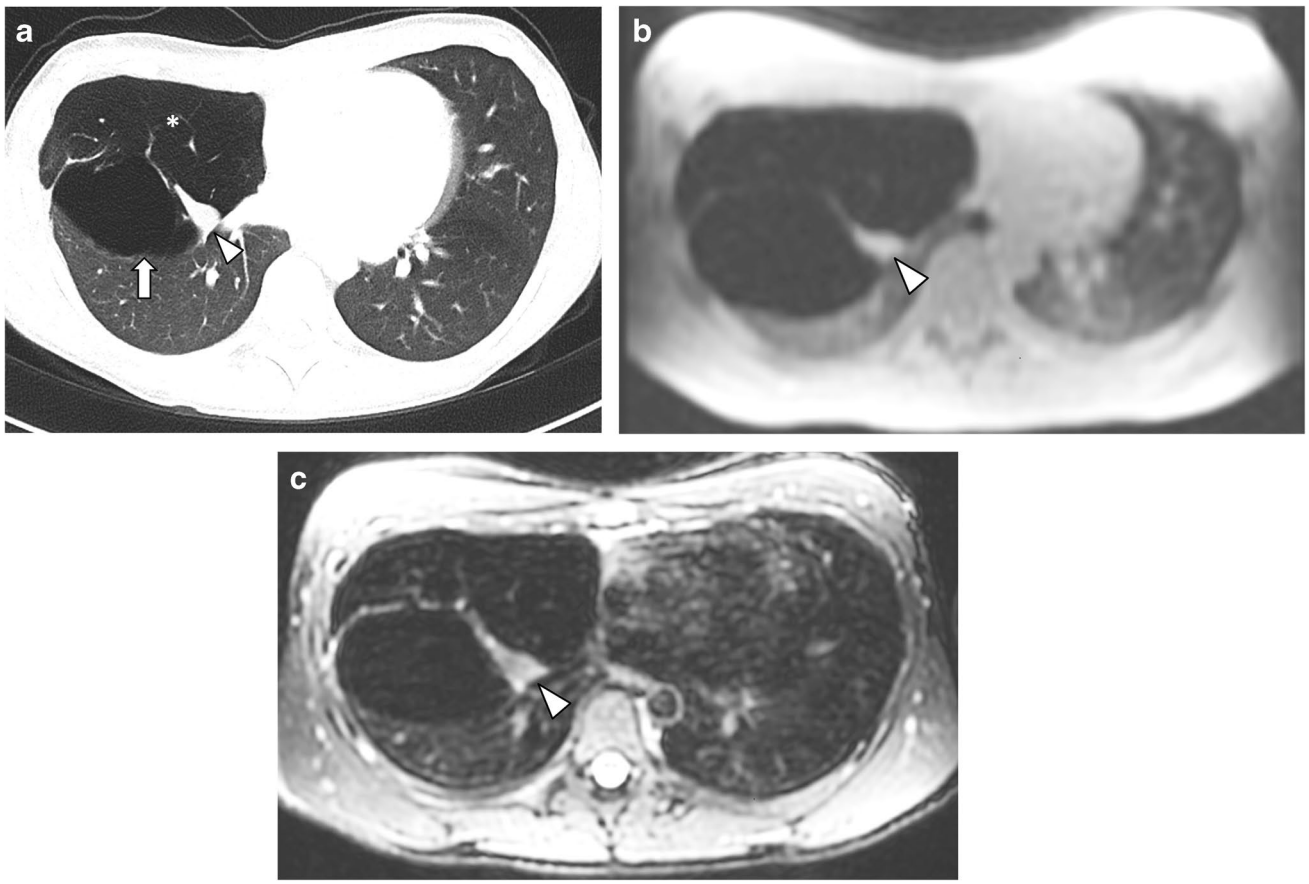

Fig. 7 Bronchial atresia and congenital lobar hyperinflation in a 16-year-old boy who presented with exercise-induced shortness of breath and respiratory distress. **a** Axial lung window CT image shows a bronchocele (*arrowhead*), bulla (*arrow*) and hyperinflated portion of lung (*asterisk*). **b, c** Axial expiratory proton-density-weighted MR image (**b**) and expiratory three-dimensional proton-density-weighted MR image (**c**) demonstrate increased signal intensity of the bronchocele component (*arrowhead*) in addition to air trapping and bulla in the lung distal to the bronchocele

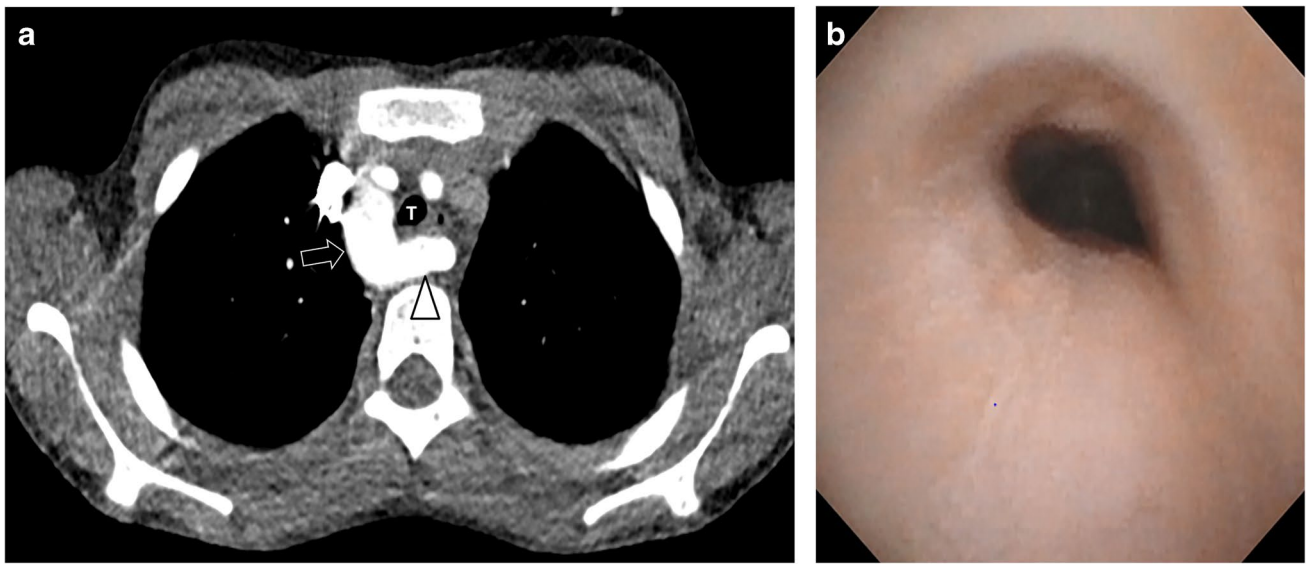

Fig. 8 Vascular ring caused by right aortic arch with an aberrant left subclavian artery in a 5-year-old girl who presented with respiratory and feeding difficulty. **a** Axial enhanced CT image shows a right-side aortic arch (*arrow*) with an aberrant left subclavian artery (*arrowhead*) resulting in tracheal narrowing (*T*). **b** Bronchoscopy confirms loss of the normal rounded contour of the trachea from posterior impression by the aberrant left subclavian artery causing tracheal narrowing

Symptoms of respiratory distress and stridor are typically correlated with the degree of airway narrowing, and dysphagia can occur when a vascular ring compresses the esophagus.

Vascular rings and pulmonary sling might be initially suspected on radiography or fluoroscopy, especially in cases with abnormal aortic arch compressing the airway. Echocardiography in the fetal and neonatal periods is often used to diagnose vascular rings and sling, but this is limited, especially in older children, by poor sonographic windows [30]. Contrast-enhanced CT angiography is the preferred test for definitive diagnosis of suspected vascular rings or pulmonary sling given its superior utility for visualizing the vascular anomaly and associated airway narrowing, often without the need for sedation. At many institutions, contrast-enhanced and non-contrast-enhanced MR angiography is becoming the preferred modality for diagnosing vascular rings and pulmonary sling for its lack of ionizing radiation. As described, sedation is often required for MR angiography in young children, and, consequently, the risks of anesthesia must be weighed against the benefits of limiting ionizing radiation when considering CT angiography versus MR angiography [7].

Acquired large airway disorders

Disorders of the large airway can be acquired, for example secondary to trauma, infection or neoplasm. Depending on the specific condition, most acquired large airway disorders are best diagnosed with static imaging protocols.

Post-traumatic large airway disorders

Post-traumatic disorders of the airway can occur from iatrogenic injury, blunt trauma or penetrating trauma. The most common post-traumatic disorders include tracheal stenosis and tracheobronchial laceration. *Tracheal stenosis* is most often related to intubation or tracheostomy tube and occurs more frequently in children with a history of multiple endotracheal intubations, prolonged endotracheal intubation, or endotracheal intubation with an inappropriately large tube [32] (Fig. 9). Tracheal stenosis can be associated with symptoms of respiratory distress and stridor, which correlate with the degree of narrowing. Acquired tracheal stenosis results in tracheal luminal caliber narrowing, which can be seen on radiography but is best assessed on CT or MRI. *Tracheobronchial laceration* can be iatrogenic, most often a complication of bronchoscopy, or non-iatrogenic and post-traumatic (e.g., high-energy trauma) [33]. Tracheobronchial laceration typically presents with dyspnea and stridor and subcutaneous emphysema, which might be evident as crepitus on physical examination. Typical findings on radiography include pneumomediastinum, subcutaneous emphysema, pneumothorax and fallen lung sign. CT is often needed to clearly delineate the site of injury [33] (Fig. 10).

Infectious large airway disorders

Various infections can affect the pediatric large airway. The most common infectious large airway disorder in the pediatric population is tuberculosis (TB) caused by *Mycobacterium tuberculosis* [5, 34] (Fig. 11). Large airway abnormality from TB infection in infants and children is typically caused by enlarged mediastinal lymphadenopathy with associated extrinsic large airway compression and subsequent narrowing. Accurate recognition of the typical low attenuation (on CT) and/or calcified mediastinal lymphadenopathy often associated with TB infection can be helpful for timely and accurate diagnosis, although a definitive diagnosis of TB is made by identifying *Mycobacterium tuberculosis* in a clinical sample (e.g., sputum, pus or tissue biopsy). Mediastinal fibrosis, which can be idiopathic or a sequela with histoplasmosis infection, can also result in pediatric large airway abnormalities; however, these are much less common than TB-related pediatric large airway abnormalities globally [5, 34].

Neoplastic large airway disorders

Primary large airway neoplasms are relatively rare in the pediatric population. Because of their rarity and often non-specific presenting symptoms, diagnosis is often missed or substantially delayed. Two primary pediatric large airway neoplasms with characteristic imaging findings are hemangioma and carcinoid tumor [5, 34] (Fig. 12). Both primary large airway neoplasms are highly vascular tumors with marked contrast enhancement. In addition, the patient age at onset and location within the large airway can be helpful imaging clues for accurate diagnosis of these primary airway neoplasms. Hemangioma, which is a benign tumor, typically occurs in infants and neonates in the subglottic region. In contrast, carcinoid tumor, which is the most common primary malignant large airway neoplasm in the pediatric population, typically occurs in adolescents in the bronchi. While large airway hemangioma in infants and neonates might spontaneously involute, carcinoid tumor requires surgical resection [5, 34].

Dynamic imaging evaluation

Tracheobronchomalacia is a condition in which the integrity of the trachea or bronchi is compromised by intrinsic weakness in the airway wall or chronic external compression, chronic inflammation, trauma or infection, leading to airway collapse when

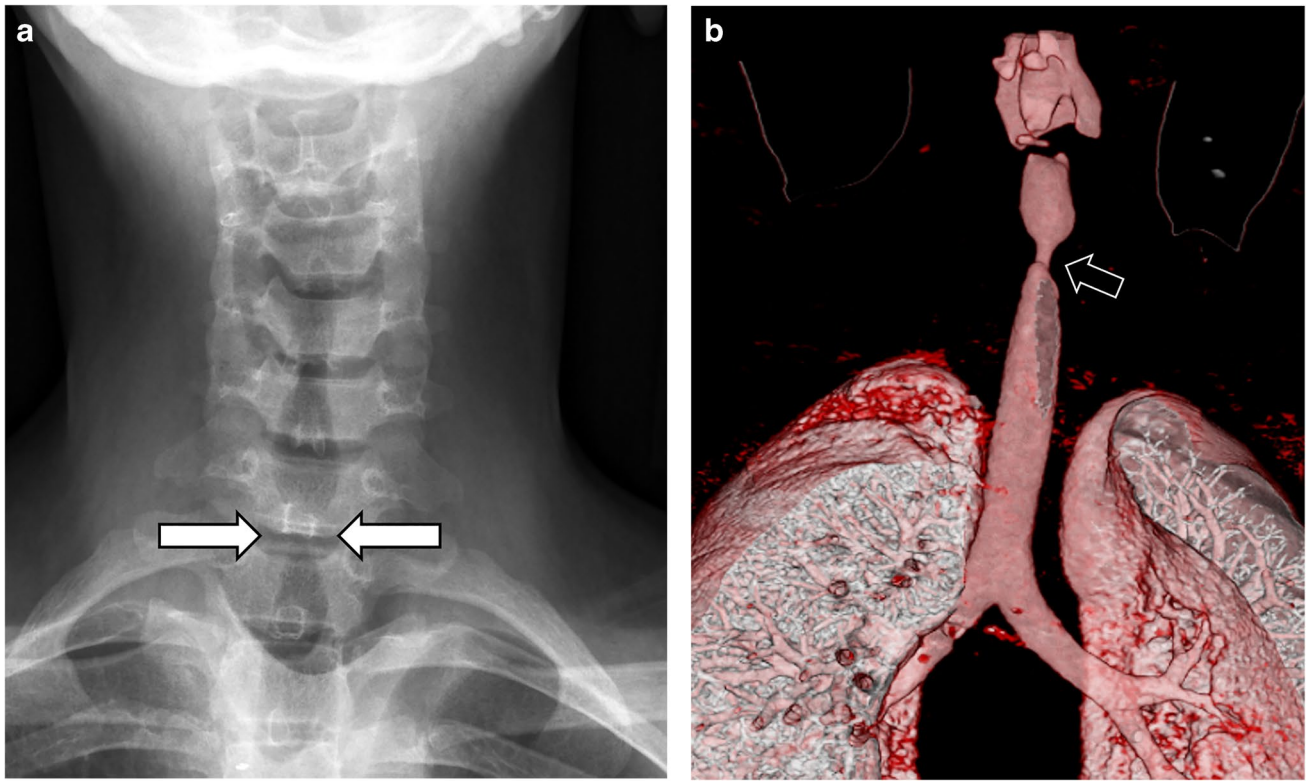

Fig. 9 Acquired tracheal stenosis in a 17-year-old girl who presented with progressively worsening shortness of breath after long-term placement of an endotracheal tube following a motor vehicle accident. **a** Anteroposterior soft-tissue neck radiograph shows narrowing of the trachea (*arrows*). **b** Anterior 3-D-volume rendered CT image shows a high-grade short-segment tracheal stenosis in the subglottic region (*arrow*)

intrathoracic pressure becomes positive during the expiratory phase of the respiratory cycle [10, 34]. Three types of tracheobronchomalacia are described [35]. Type I (also known as primary tracheobronchomalacia) is characterized by excessive collapse of the large airway during expiration in the absence of an abnormal structure causing extrinsic compression. Type II is characterized by extrinsic compression of the large airway by a vascular anomaly, such as a vascular rings or pulmonary sling, chest wall deformity or intrathoracic mass. Type III is characterized by acquired large airway damage caused by mechanical ventilation, tracheostomy or an inflammatory condition. These children might experience symptoms of respiratory distress and expiratory stridor from excessive collapse of the large airway during expiration.

In tracheobronchomalacia, the large airway is often normal in caliber during inspiration, when negative intrathoracic pressure helps to hold the airway open. Consequently, tracheobronchomalacia is often missed on standard single end-inspiratory-phase imaging. Because the abnormality in tracheobronchomalacia is dynamic and typically only visible in the expiratory phase, dynamic imaging through both inspiration and expiration is required for diagnosis (Fig. 13).

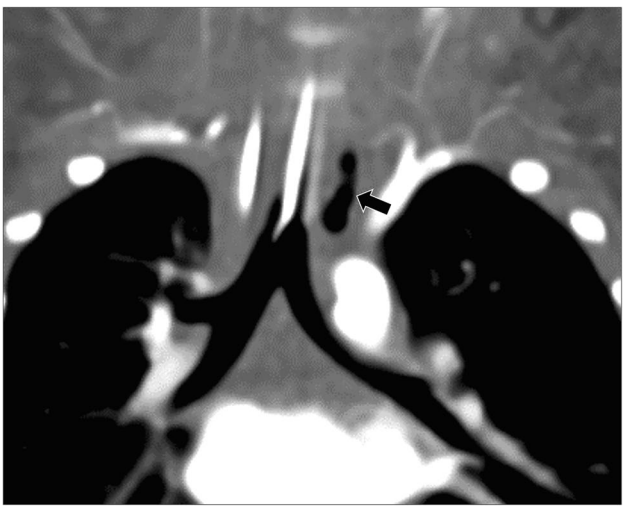

Fig. 10 Tracheal laceration in a 3-month-old girl who underwent multiple attempts at endotracheal tube placement. Coronal enhanced CT image shows mediastinal air (*arrow*) adjacent to the left side of the trachea with an endotracheal tube placement. Subsequently obtained bronchoscopy showed a tracheal laceration

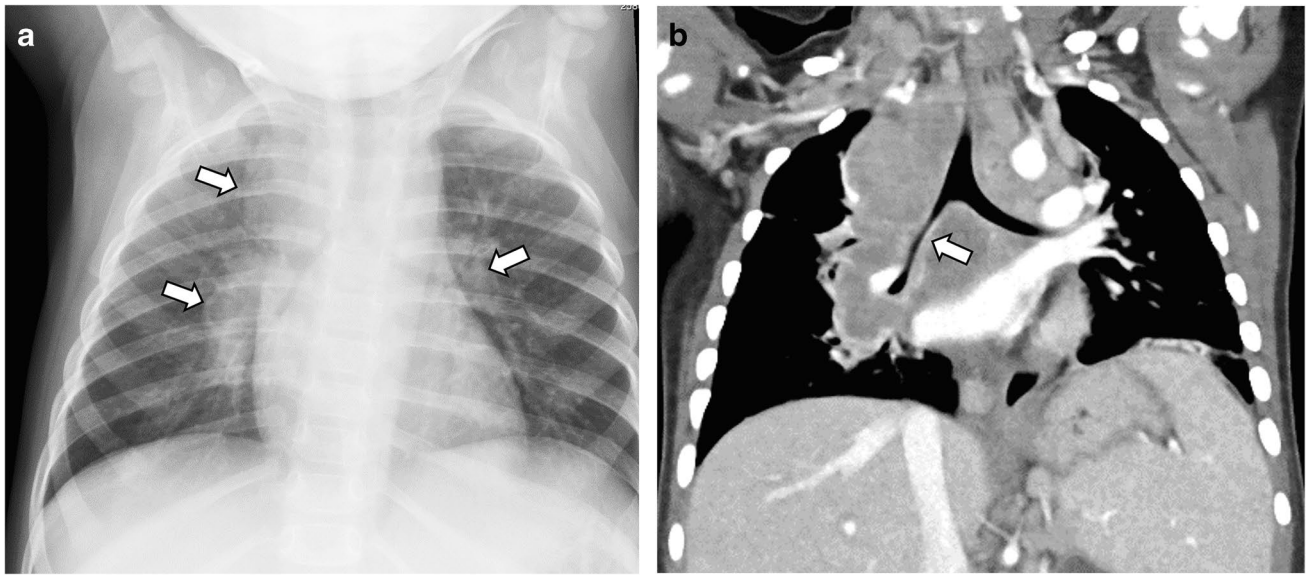

Fig. 11 Tuberculosis-infection-associated large airway narrowing in an 18-month-old girl who presented with fever, cough and weight loss. **a** Anteroposterior chest radiograph shows an enlarged mediastinal contour (*arrows*) suspicious for underlying lymphadenopathy. **b** Coronal enhanced CT image demonstrates mediastinal lymphadenopathy with areas of low attenuation and associated right-side bronchial narrowing (*arrow*)

Imaging protocols might include two-phase static imaging (e.g., end-inspiration and end-expiration), cine imaging during free breathing, and 4-D dynamic CT imaging during free breathing where a three-dimensional (3-D) rendering of the large airway is imaged through time [6, 7, 10, 15, 34, 36]. Although bronchoscopy is the gold standard for the diagnosis, dynamic imaging with CT or MRI has been used with increased frequency because of the benefits of avoiding invasive bronchoscopy. At this time, CT protocols for dynamic evaluation of the large airway have been in use for a relatively long time and are well-established [5, 10, 34, 36]. MRI protocols have gained attention because of the benefit of avoiding ionizing radiation and are being used in place of CT in centers with specialized MRI expertise [7, 22, 37]. Detailed MRI protocols for dynamic large airway evaluation are shown in Tables 2 and 3.

Future directions

Diagnostic imaging of the pediatric large airway has undergone a major evolution from radiography to modern cross-sectional evaluation of the pediatric large airway during multiple phases of the respiratory cycle with 3-D or 4-D reformations utilizing CT and MRI. Refinement of MR imaging techniques to allow imaging without motion artifact and eliminate the need for sedation in children is an important area of future development.

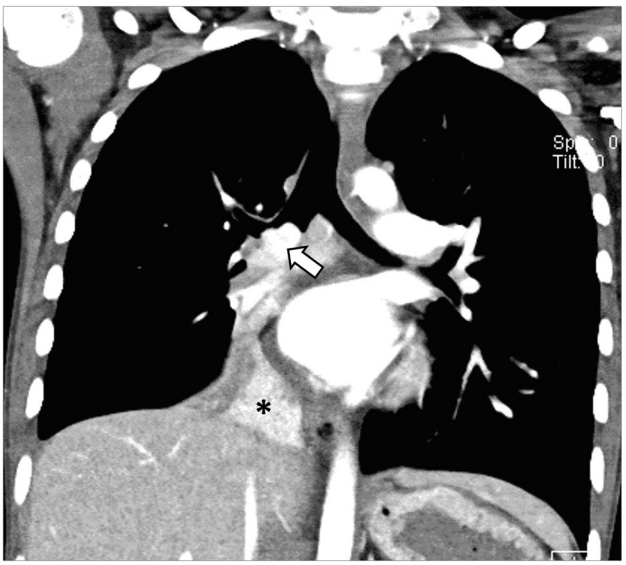

Fig. 12 Carcinoid tumor in a 7-year-old girl who presented with progressively worsening respiratory distress and right-side chest pain. Axial enhanced CT image shows a markedly enhancing endobronchial tumor (*arrow*) causing right lower lobe atelectasis (*asterisk*). Surgical pathology confirmed the diagnosis of carcinoid tumor

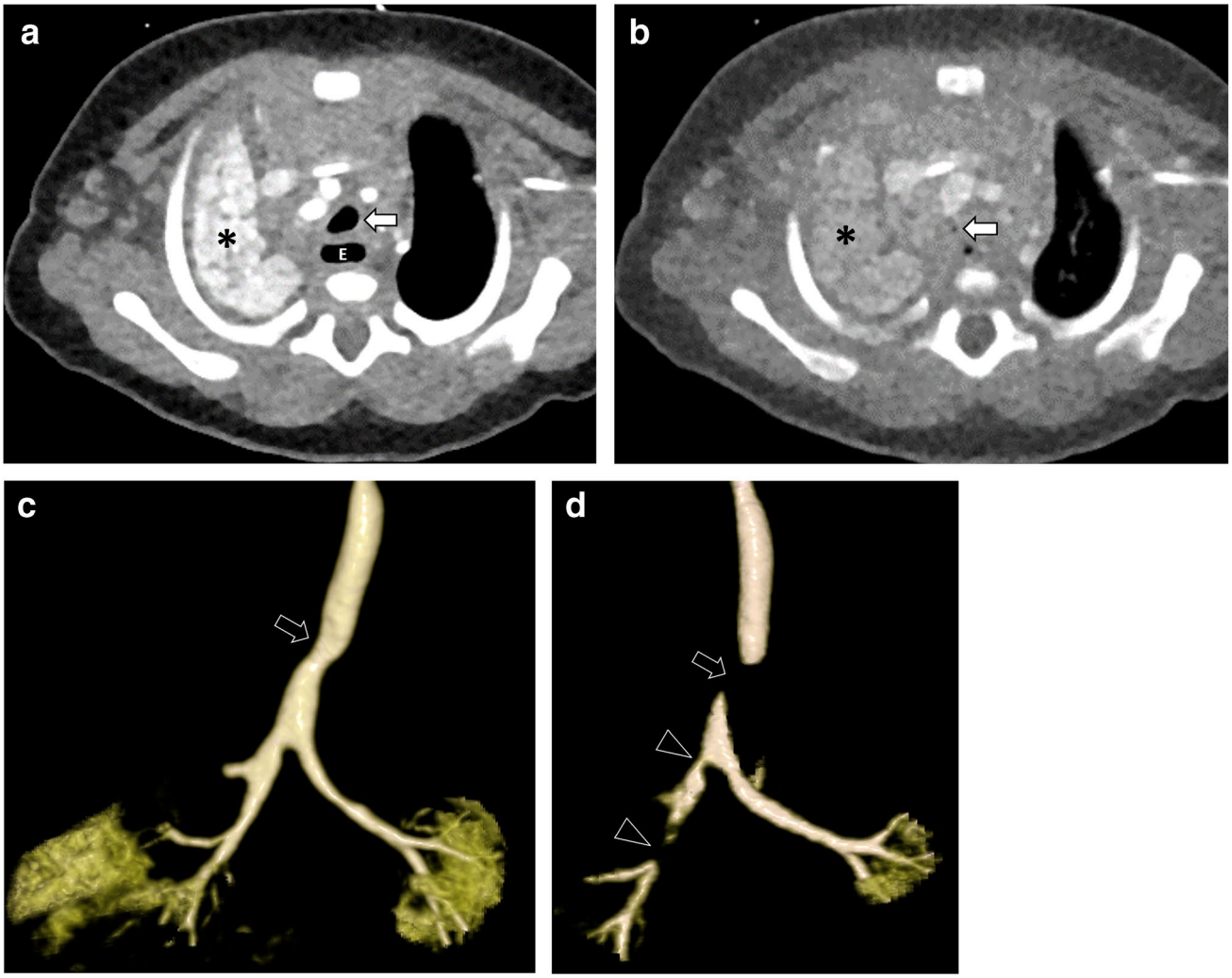

Fig. 13 Tracheomalacia in a 4-month-old boy who presented with cough and respiratory distress. **a** Axial enhanced CT image obtained with respiration suspended at end-inspiration shows a patent but mildly narrowed trachea (*arrow*). Right upper lobe atelectasis (*asterisk*) is also seen. *E* esophagus. **b** Axial enhanced CT image obtained with respiration suspended at end-expiration demonstrates a complete collapse of the trachea (*arrow*), consistent with tracheomalacia. Note also the right upper lobe atelectasis (*asterisk*). **c** Anterior 3-D-volume rendered CT image obtained with respiration suspended at end-inspiration shows a patent but mildly narrowed trachea (*arrow*). **d** Anterior 3-D-volume rendered CT image obtained with respiration suspended at end-expiration demonstrates a completely collapsed trachea (*arrow*), consistent with tracheomalacia. The longitudinal extent of the tracheomalacia is better visualized on the 3-D CT reconstructed image than the axial CT image. Of note, multifocal right main bronchus and bronchus intermedius bronchomalacia (*arrowheads*) is also seen

Conclusion

Airway imaging is frequently performed to evaluate respiratory symptoms in children and infants. It is essential that radiologists be familiar with the variety of imaging modalities and techniques, as well as characteristic imaging findings of pediatric airway disorders, so they can make timely and accurate diagnoses to guide appropriate management.

Acknowledgments The authors would like to thank Piotr A. Wielopolski, PhD, for providing information included in Tables 1, 2 and 3.

Declarations

Conflicts of interest MCL is the recipient of grant funding for unrelated study from Carestream Health, Inc., is an unpaid member of of Carestream Health Medical Advisory Board, and recipient of travel and meal support from Carestream Health.

References

1. Baez JC, Ciet P, Mulkern R et al (2015) Pediatric chest MR imaging: lung and airways. Magn Reson Imaging Clin N Am 23:337–349
2. Isaiah A, Pereira KD (2017) Laryngotracheal anomalies and airway fluoroscopy in infants. Int J Pediatr Otorhinolaryngol 97:109–112
3. Wallis C, Alexopoulou E, Antón-Pacheco JL et al (2019) ERS statement on tracheomalacia and bronchomalacia in children. Eur Respir J 54:1900382
4. Ngerncham M, Lee EY, Zurakowski D et al (2015) Tracheobronchomalacia in pediatric patients with esophageal atresia: comparison of diagnostic laryngoscopy/bronchoscopy and dynamic airway multidetector computed tomography. J Pediatr Surg 50:402–407
5. Lee EY, Greenberg SB, Boiselle PM (2011) Multidetector computed tomography of pediatric large airway diseases: state-of-the-art. Radiol Clin North Am 49:869–893
6. Lee EY, Zucker EJ, Restrepo R et al (2013) Advanced large airway CT imaging in children: evolution from axial to 4-D assessment. Pediatr Radiol 43:285–297
7. Liszewski MC, Ciet P, Lee EY (2019) MR imaging of lungs and airways in children: past and present. Magn Reson Imaging Clin N Am 27:201–225
8. Liszewski MC, Ciet P, Sodhi KS, Lee EY (2017) Updates on MRI evaluation of pediatric large airways. AJR Am J Roentgenol 208:971–981
9. Yedururi S, Guillerman RP, Chung T et al (2008) Multimodality imaging of tracheobronchial disorders in children. Radiographics 28:e29
10. Lee EY, Boiselle PM (2009) Tracheobronchomalacia in infants and children: multidetector CT evaluation. Radiology 252:7–22
11. Tivnan P, Winant AJ, Johnston PR et al (2021) Thoracic CTA in infants and young children: image quality of dual-source CT (DSCT) with high-pitch spiral scan mode (turbo flash spiral mode) with or without general anesthesia with free-breathing technique. Pediatr Pulmonol 56:2660–2667
12. Long FR, Castile RG (2001) Technique and clinical applications of full-inflation and end-exhalation controlled-ventilation chest CT in infants and young children. Pediatr Radiol 31:413–422
13. Goo HW (2019) Four-dimensional thoracic CT in free-breathing children. Korean J Radiol 20:50–57
14. Goo HW (2013) Free-breathing cine CT for the diagnosis of tracheomalacia in young children. Pediatr Radiol 43:922–928
15. Lee EY, Strauss KJ, Tracy DA et al (2010) Comparison of standard-dose and reduced-dose expiratory MDCT techniques for assessment of tracheomalacia in children. Acad Radiol 17:504–510
16. Greenberg SB, Dyamenahalli U (2014) Dynamic pulmonary computed tomography angiography: a new standard for evaluation of combined airway and vascular abnormalities in infants. Int J Cardiovasc Imaging 30:407–414
17. Ciet P, Tiddens HA, Wielopolski PA et al (2015) Magnetic resonance imaging in children: common problems and possible solutions for lung and airways imaging. Pediatr Radiol 45:1901–1915
18. Baez JC, Seethamraju RT, Mulkern R et al (2015) Pediatric chest MR imaging: sedation, techniques, and extracardiac vessels. Magn Reson Imaging Clin N Am 23:321–335
19. Salamon E, Lever S, Kuo W et al (2017) Spirometer guided chest imaging in children: it is worth the effort! Pediatr Pulmonol 52:48–56
20. Puderbach M, Hintze C, Ley S et al (2007) MR imaging of the chest: a practical approach at 1.5 T. Eur J Radiol 64:345–355
21. Tan JZ, Crossett M, Ditchfield M (2013) Dynamic volumetric computed tomographic assessment of the young paediatric airway: initial experience of rapid, non-invasive, four-dimensional technique. J Med Imaging Radiat Oncol 57:141–148
22. Faust RA, Remley KB, Rimell FL (2001) Real-time, cine magnetic resonance imaging for evaluation of the pediatric airway. Laryngoscope 111:2187–2190
23. Ciet P, Wielopolski P, Manniesing R et al (2014) Spirometer-controlled cine magnetic resonance imaging used to diagnose tracheobronchomalacia in paediatric patients. Eur Respir J 43:115–124
24. Biyyam DR, Chapman T, Ferguson MR et al (2010) Congenital lung abnormalities: embryologic features, prenatal diagnosis, and postnatal radiologic-pathologic correlation. Radiographics 30:1721–1738
25. Desir A, Ghaye B (2009) Congenital abnormalities of intrathoracic airways. Radiol Clin North Am 47:203–225
26. Berdon WE, Muensterer OJ, Zong YM, Backer CL (2012) The triad of bridging bronchus malformation associated with left pulmonary artery sling and narrowing of the airway: the legacy of Wells and Landing. Pediatr Radiol 42:215–219
27. Hewitt RJ, Butler CR, Maughan EF, Elliott MJ (2016) Congenital tracheobronchial stenosis. Semin Pediatr Surg 25:144–149
28. Uchida DA, Morgan-Wallace V, Richards K et al (2009) Congenital tracheal stenosis masquerading as asthma in an adolescent: the value of spirometry. Clin Pediatr 48:432–434
29. Kellenberger CJ, Amaxopoulou C, Moehrlen U et al (2020) Structural and perfusion magnetic resonance imaging of congenital lung malformations. Pediatr Radiol 50:1083–1094
30. Kussman BD, Geva T, McGowan FX (2004) Cardiovascular causes of airway compression. Paediatr Anaesth 14:60–74
31. Berdon WE, Baker DH, Wung JT et al (1984) Complete cartilage-ring tracheal stenosis associated with anomalous left pulmonary artery: the ring-sling complex. Radiology 152:57–64
32. Downing GJ, Kilbride HW (1995) Evaluation of airway complications in high-risk preterm infants: application of flexible fiberoptic airway endoscopy. Pediatrics 95:567–572
33. Moser JB, Stefanidis K, Vlahos I (2020) Imaging evaluation of tracheobronchial injuries. Radiographics 40:515–528
34. Lee EY, Litmanovich D, Boiselle PM (2009) Multidetector CT evaluation of tracheobronchomalacia. Radiol Clin North Am 47:261–269
35. Carden KA, Boiselle PM, Waltz DA, Ernst A (2005) Tracheomalacia and tracheobronchomalacia in children and adults: an in-depth review. Chest 127:984–1005
36. Lee EY, Siegel MJ (2007) MDCT of tracheobronchial narrowing in pediatric patients. J Thorac Imaging 22:300–309
37. Ciet P, Boiselle PM, Heidinger B et al (2017) Cine MRI of tracheal dynamics in healthy volunteers and patients with tracheobronchomalacia. AJR Am J Roentgenol 209:757–761